Journal of Materials Chemistry A

Accepted Manuscript

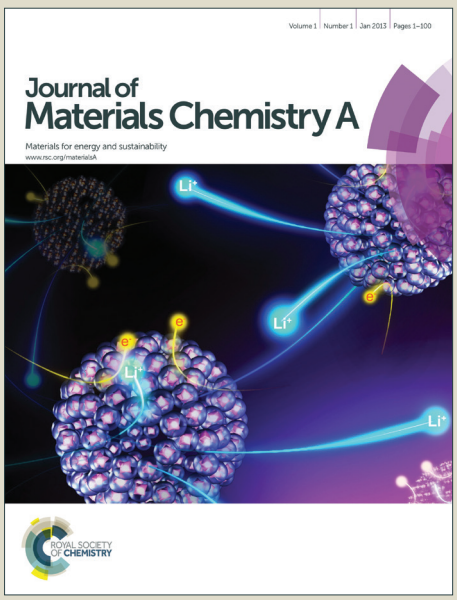

ROYAL SOCIETY OF CHEMISTRY

www.rsc.org/materialsA

Cite this: DOI: 10.1039/c0xx00000x

www.rsc.org/xxxxxx

ARTICLE TYPE

Effect of depositing silver nanoparticles on $BiVO_4$ in enhancing visible light photocatalytic inactivation of bacteria in water†

Amin Yoosefi Booshehri,[a,b] Simon Chun-Kiat Goh,[a] Jindui Hong,[a] Rongrong Jiang,[a] and Rong Xu*[a]

Received (in XXX, XXX) XthXXXXXXXXX 20XX, Accepted Xth XXXXXXXXX 20XX

DOI: 10.1039/b000000x

Recently photocatalytic processes have been shown to be a promising low-cost and sustainable alternative for water and wastewater treatment. In this study $Ag/BiVO_4$ composites were fabricated and their photocatalytic disinfection activity was tested against *Escherichia coli* under visible light ($\lambda > 420$ nm). Deposition of silver nanoparticles on the surface of $BiVO_4$ showed significant improvement on the photocatalytic activity. Irradiation of the suspension of *Escherichia coli* (10^7 CFU/mL) in the presence of $Ag/BiVO_4$ resulted in total disinfection of the cells within 3 h. Photocatalytic activity of the composite was stable in repeated runs. The disinfection study was also conducted under the tropical afternoon Sun in Singapore. The significant enhancement in the photocatalytic activity of $Ag/BiVO_4$ can be ascribed to the effect of metallic silver nanoparticles which act as an electron trap on the surface of $BiVO_4$ and promote separation of photo-induced electron/hole pairs for the generation of reactive oxygen species.

Introduction

Waterborne diseases are one of the main cause of death in the world.[1] With escalating fresh water demand, this issue represents one of the most serious challenges facing mankind. Different methods such as chlorination, ozonation, UV irradiation and membrane technology are available but each of which has its own disadvantage. Water chlorination and oxidation methods produce disinfection byproducts.[2] UV disinfection is energy intensive and direct use of it is harmful.[3] Membrane technology although removes bacteria from water, it doesn't kill them. Further, after formation of biofilm on its surface, it is a source of pollution itself.[4] Using combination of sunlight and photocatalysts can be a promising alternative especially in regions with abundant sunshine but without adequate infrastructure.[5]

Photocatalytic process has been adopted as a promising way of producing pathogen-free water by Matsunaga et al. in 1985.[6] Since then many researchers have studied photocatalytic disinfection of water.[7] Besides fundamental studies, both engineering and economical feasibilities of the photocatalytic water treatment systems have been explored. Although they are not in widespread use yet, there are examples of successful pilot plants[8-11] in which TiO_2 was mostly used.

However, TiO_2 due to its wide band gap can only absorb UV light which accounts for around 5% of the solar energy. Although modification of TiO_2 can extend its application to visible light region, it often leads to complicated fabrication processes.[12] Hence, photocatalysts that are inherently visible light responsive and can be prepared by simple methods are preferred.

The main mechanism of antibacterial activity of semiconductor particles is attributed to the oxidative stress caused by the production of reactive oxygen species (ROS).[13] ROS are highly reactive oxygen-containing species which can result in significant damage to cell due to destruction of cell membranes.[14] Photogenerated electrons (e^-) and holes (h^+) upon migrating to the surface of semiconductor particles can react with dissolved oxygen and water molecules, respectively to produce superoxide anion ($O_2^{\bullet-}$) and hydroxyl radical (•OH) through a reduction and oxidation reaction.[13] Singlet oxygen ($^1O_2$) can also be produced indirectly from aqueous reaction of superoxide anion.[15] All three of these species which are known as ROS can irreversibly damage biomolecules and inactivate bacteria.[13]

Among visible light active photocatalysts, bismuth vanadate ($BiVO_4$) has received good attention.[16-18] $BiVO_4$ has three main crystal structures including tetragonal zircon, tetragonal scheelite and monoclinic scheelite. $BiVO_4$ of monoclinic scheelite phase has a band gap of 2.4 eV and has been demonstrated with much higher photocatalytic activity than the other two phases.[19] Micro-sized $BiVO_4$ particles of good crystallinity can be readily produced by a homogeneous precipitation method and used in water purification process since they can be separated easily.[20] However, the photoactivity of $BiVO_4$ alone is not very impressive because of a relatively fast recombination of photogenerated electron-hole pairs.[17] One of the most effective way of improving the photocatalyst performance is by depositing metal nanoparticles on the surface of the semiconductor.[17] These metal nanoparticles can act as a sink for photo-induced electrons, thus facilitating the charge separation and enhancing the photocatalytic activity.[21] So far, various noble metals have been deposited on semiconductors to improve the photoactivity such as Pt, Au, Ag, etc.[22-24] Among them Ag has been well studied in the systems including Ag/TiO_2, Ag/AgCl, Ag/ZnO and $Ag/BiVO_4$.[25-28] It has been shown that

[a]*School of Chemical & Biomedical Engineering, Nanyang Technological University, 62 Nanyang Drive, Singapore 637459. Fax: 65-67947553; Tel: 65-67906713; E-mail: rxu@ntu.edu.sg*

[b]*Singapore Membrane Technology Centre, Nanyang Environmental and Water Research Institute, 1 Cleantech Loop, Singapore 617141*

surface deposited silver nanoparticles greatly enhance the photocatalytic activity under visible light.[25, 27]

To the best of our knowledge, study on water disinfection with $BiVO_4$ has only been reported by Wang *et al*. who investigated the antibacterial activity of $BiVO_4$ nanotubes alone under visible light.[18] Photocatalytic applications of $BiVO_4$ deposited with silver nanoparticles are only limited to dye degradation and water splitting so far.[20,25,29] However, bacteria inactivation is attributed to the oxidation/damage of the organic molecules of their cellular membrane and the nucleic acids of their DNA. Bacteria are living species which are designed to survive even in harsh environment.[30] Firstly, they have a defense mechanism that makes them to be able to resist against oxidative agents[31] and secondly even if the damage occurs they may have a system to repair it and maintain their viability.[32] In the present study, silver was photoreduced on the surface of $BiVO_4$ crystal. Hence, silver nanoparticles are exposed on the active site of the photocatalyst to capture photo-induced electrons. We conducted systematic study on the effect of silver loading coupled with the measurement of free radical concentrations. The resultant photocatalyst with the optimum loading of silver leads to total disinfection of *Escherichia coli* (*E. coli)* in water within a relatively short time duration. Outdoor tests under natural tropical sunlight were also performed, further indicating the feasibility of applying such a photocatalytic water disinfection system by utilizing sustainable solar energy.

Experimental section

Materials

$Bi(NO_3)_3{\cdot}5H_2O$ (98%), NH_4VO_3 (99%), $AgNO_3$ (99+%) and disodium terephthalate (TPA) were purchased from Alfa Aeser. HNO_3 (69+% of aqueous solution) was supplied by Fluka and urea from Bio-RAD. Nitrotetrazolium blue (NBT) (98%) was purchased from Sigma Aldrich. Luria-Bertani (LB) broth (Difco LB Broth, Miller) from BD (Becton, Dickinson and Company), HEPES buffer solution from PAA and α-D-Glucose from Aldrich were used to make the bacterial solution. *E. coli* (ATCC8739) was used as the model bacterium. Throughout the experiments, deionized water was used.

Preparation of $BiVO_4$ and Ag/$BiVO_4$

$BiVO_4$ was synthesized by a homogeneous precipitation method followed by aging at 80 ºC.[33] Briefly, 6 mmol of $Bi(NO_3)_3{\cdot}5H_2O$ was dissolved in 32 mL of 1M HNO_3 aqueous solution under stirring until a clear solution was formed. Then an equal mole of NH_4VO_3 was added to this solution. After the color of the mixture was changed to yellowish orange, 3.0 g of urea was added and the mixture was then heated to 80 ºC and kept at this temperature for 24 h. The resultant precipitate was washed thoroughly with deionized water until the pH of the supernatant solution was reached around 7.0. The washed sample was dried in oven at 60 ºC overnight.

Silver nanoparticles were loaded on $BiVO_4$ by a photodeposition method. The as-prepared $BiVO_4$ (100 mg) was dispersed in 50 mL of deionized water and then a certain amount of $AgNO_3$ was added. The mixture was irradiated by a Xe lamp (300 W, $\lambda > 420$ nm by equipping a long-pass cut-off filter) for 1 h. The resultant sample was washed thoroughly with deionized water and dried in a freeze drier overnight.

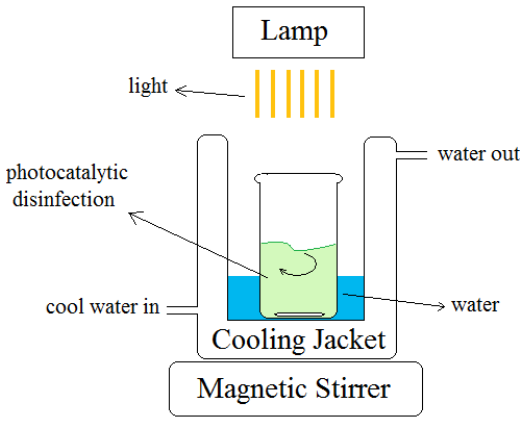

Figure 1. Schematic diagram of the photocatalytic disinfection set-up.

Characterization

The crystal structures of the samples were analyzed by powder X-ray diffraction (XRD) on a Bruker AXS D8 X-ray diffractometer with Cu Kα radiation (λ = 1.5406 Å) at 40 kV and 20 mA. X-ray photoelectron spectroscopy (XPS) analysis was carried out on a VG Escalab 220i XL. The binding energy was calibrated using C1s at 285.0 eV which is originated from the adventitious carbon. UV-visible diffuse reflectance spectroscopy (DRS) results were obtained on a UV-Vis spectrophotometer (Shimadzu UV-2450). Fluorescence measurements were conducted on a PerkinElmer LS 55 Fluorescence Spectrometer. The morphologies of the particles and bacteria cells after disinfection were analyzed with FESEM (JEOL JSM 6700F field emission). The average size of silver nanoparticles was obtained by measuring the sizes of 50 silver nanoparticles during FESEM analysis. To prepare samples of bacteria for FESEM observation, 2 mL of the reaction and control medium was collected, centrifuged and washed with deionized water. Then 5 µL of the mixture was dropped on a slide and dried in the freeze drier. The control sample was taken from a parallel test with the same condition as the disinfection test but without catalyst or light. The percentage of silver in Ag/$BiVO_4$ samples and the concentration of silver ions in disinfection medium were determined by inductively coupled plasma atomic emission spectroscopy (ICP-AES) on a Perkin Elmer ICP Optima 2000DV. When measuring the concentration of silver ions in the reaction medium after the tests, 9.8 mL of the reaction mixture was collected and filtered to remove the solid particles. The liquid sample was added with 200 µL of HNO_3 aqueous solution (10 vol%) before the test. For measuring the percentage of silver in the composite, 20 mg of the solid sample was dispersed in 10 mL of HNO_3 solution (10 vol%) and shaken for 24 h. The mixture was then filtered to remove the solid $BiVO_4$ particles.

Photocatalytic disinfection tests

E. coli was used as a model bacterium to investigate the antimicrobial activity of $BiVO_4$ and Ag/$BiVO_4$. All glasses and materials were sterilized at 121 ºC for 30 min in an autoclave. The bacterial cells were cultured to a mid-log phase in Luria-Bertani (LB) broth at 37 ºC. The cells were then separated by centrifugation, washed and re-suspended in a mixture solution of HEPES buffer (10 mM) and glucose (1 wt%) with the cell concentration kept approximately at 10^7 colony forming units (CFU) per mL. The photocatalytic disinfection was carried out in a

system schematically shown in Figure 1. It consists of a Xe lamp equipped with a long-pass cut-off filter (300 W, $\lambda > 420$ nm) as visible light source, a batch Pyrex glass reactor, and double walled glass cooling jacket with circulating water maintained at 20 ^{o}C. During each test, 30 mL of bacterial suspension added with the solid photocatalyst at 2 mg/mL was continuously stirred. To monitor the disinfection process, at certain time interval, 100 µL of the suspension was collected for analysis. The concentration of the cells in the mixture was analyzed by the plate counting technique. Cells were cultured on a nutrition agar medium at 37 ^{o}C for 24 h and then the number of cells was counted based on colonies formed on the plate. At the end of each run, the concentration of silver ions in the solution was measured by ICP method. The disinfection test was also carried out with natural sunlight under the partly cloudy afternoon sky on May 18th, 19th and 20th 2013 on Nanyang Technological University campus in Singapore (1º 20' 43" N 103º 40' 44" E), while keeping other conditions the same as those during the lab tests. The stability of Ag/$BiVO_4$ was evaluated by recycling the sample. After each disinfection test, the sample was collected by centrifugation, washed with deionized water and then dried in a freeze drier overnight before the next run.

Quantification of hydroxyl radical (•OH) and superoxide anion (O_2•$^-$)

Terephthalate (TPA) was used as a probe for hydroxyl radical detection. TPA itself has no fluorescence property. After absorption of •OH, it forms hydroxyterephthalate (hTPA) which has a fluorescence signal at around 425 nm by excitation at 315 nm.[34,35] The experimental condition of detecting hydroxyl radical was the same as that of antibacterial test except in the absence of bacterial cells. Briefly, 30 mL of an aqueous solution of TPA (5 mM) containing 2 mg/mL of the catalyst was irradiated for 30 min. The solid was then separated by centrifugation and the supernatant was used for fluorescence spectroscopy analysis. In the control test, the same process was carried out except without the catalyst. Nitroblue tetrazolium (NBT) which can be reduced by O_2•$^-$ was used as the probe for superoxide anion detection. During the process, 0.15 mM of aqueous solution of NBT solution was used. The other conditions were kept the same as those for hydroxyl radical detection. The production of O_2•$^-$ in the reaction medium was analyzed by detecting the decrease in the concentration of NBT in the supernatant solution by UV-Vis spectroscopy.[36]

Results and discussion

Properties of $BiVO_4$ and Ag/$BiVO_4$

Figure 2 shows the FESEM images of as-prepared $BiVO_4$ particles at different magnifications. It can be observed that the particles exhibit a wide range of size distribution from about 0.5 to 5 µm. As observed in Figure 2D, these particles have well defined truncated octahedron shapes with smooth and highly exposed facets. Based on the studies which have been conducted on this type of $BiVO_4$ morphology, the exposed facets should be (011), (010) and (110) as shown in Figure 2D.[37,38] The most commonly used methods for synthesis of $BiVO_4$ particles are aqueous precipitation and hydrothermal methods.[39,40] In these methods, reaction conditions in particular the pH of precipitation have drastic influence on the morphology of $BiVO_4$ particles.[38] It has been observed that the photocatalytic activity of $BiVO_4$ is dependent more on the surface structure and shape than other properties like surface area.[38] Synthesis of large $BiVO_4$ particles with well faceted surfaces has been reported in the literature.[37,41,42] It has been demonstrated that the photocatalytic activity of $BiVO_4$ is highly dependent on the degree of exposure of (010) facet,[43,44] owing to its higher charge mobility and easier absorption of water.[45] It can be seen from Figure 2D that (010) facet is well exposed on the surface of as-prepared $BiVO_4$.

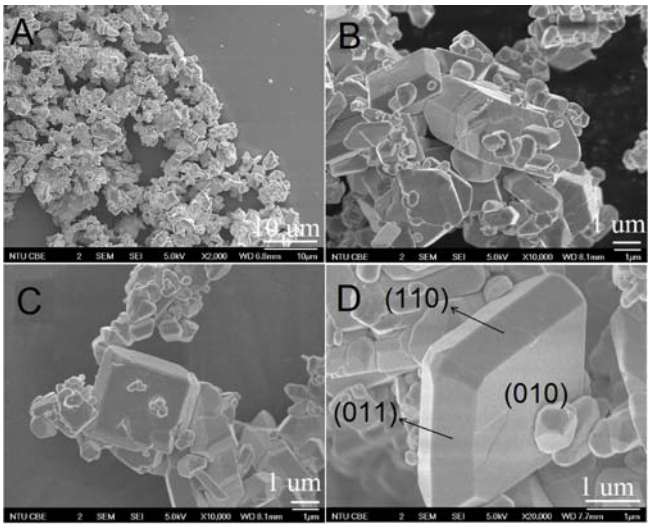

Figure 2. FESEM images of $BiVO_4$ at different magnifications.

Silver nanoparticles were photodeposited on the surface of $BiVO_4$ using $AgNO_3$ as the precursor and water as the hole (h^+) scavenger. The proposed reactions are shown in Equations 1-3. Upon exposure to light, electron (e^-)/hole (h^+) pairs are generated in $BiVO_4$ particles (Equation 1) and they are separated and then migrate to the surface of the particles. Photogenerated e^- reduces Ag^+ cations to metallic silver (Equation 2) and at the same time photogenerated h^+ is eliminated by water oxidation reaction (Equation 3).

$$BiVO_4 + h\nu \rightarrow h^+ + e^- \quad (1)$$

$$Ag^+ + e^- \rightarrow Ag \quad (2)$$

$$2H_2O + 4h^+ \rightarrow O_2 + 4H^+ \quad (3)$$

The XRD patterns of $BiVO_4$ and Ag/$BiVO_4$ are shown in Figure 3. The as-prepared $BiVO_4$ (Figure 3A) has a monoclinic structure (PDF no. 00-074-4894). After deposition of silver nanoparticles, four additional peaks at 38º, 44º, 64º and 77º appear and are readily assigned to (111), (200), (220) and (311) diffractions of face centered cubic metallic silver (PDF no. 001-1167). The weight percentage of silver in Ag/BiO_4 determined by ICP method ranges from 1.3% to 23.5%. As the silver loading was increased, their diffraction intensities increase correspondingly (Figure 3B-F). The UV-Vis absorption spectra (Figure 4) show that all samples exhibit strong absorption in the visible light region. The band gap of as-prepared $BiVO_4$ is around 2.3 eV which is consistent with the values reported in the literature.[38,41] After loading of silver, two phenomena can be observed. Firstly, the absorption in the range of 500-800 nm is significantly enhanced even at the lowest silver content of 1.3%. Upon further increasing of silver loading, the absorption in this region is further enhanced but not according to a linear fashion. In accordance with the UV-

Vis absorption results, change of the sample color from greenish yellow to dark green was observed after deposition of silver (Figure 4 inset). Secondly, the shape of the absorption edge is changed with a slight red shift. Figure 4 also indicates that the decrease in band gap energy of the photocatalyst is enhanced by the increased the silver loading. This phenomenon can be attributed to the surface plasmon resonance (SPR) effect of silver nanoparticles.[23,25,46,47] SPR effect makes the transfer of energy to semiconductor easier by three ways: red shift of the absorption wavelength, increasing light scattering, and exciting electron-hole pair by transferring plasmon energy from metal to semiconductor.[48,49]

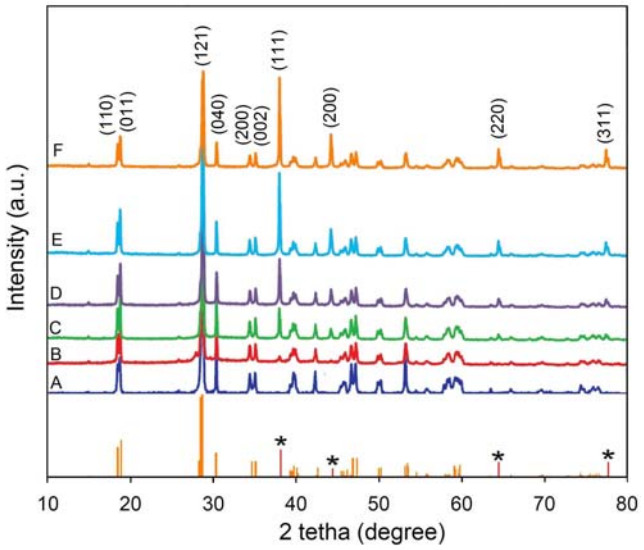

Figure 3. XRD patterns of A) $BiVO_4$, B) Ag/$BiVO_4$-1.3%, C) Ag/$BiVO_4$-6.9%, D) Ag/$BiVO_4$-12.3%, E) Ag/$BiVO_4$-19.7%, and F) Ag/$BiVO_4$-23.5%. The percentage refers to the weight percentage of silver determined by ICP method. Line patterns specified by * are attributed to cubic phased silver (PDF no. 001-1167), and the rest are corresponding to monoclinic $BiVO_4$ (PDF no. 00-074-4894).

Figure 5 shows the FESEM images of Ag/$BiVO_4$ samples. It is observed that by increasing the silver content, the surface of $BiVO_4$ is more extensively covered by silver nanoparticles. At the lower loadings of 1.3% (Figure 5B) and 6.9% (Figure 5C), silver nanoparticles tend to deposit more on the (010) facet of the crystal. At higher loadings, the sizes of silver nanoparticles become bigger and they can also be observed on the other facets (Figure 5D-F). With a loading of 1.3 wt%, the average size of the nanoparticles is around 13 nm and it increases to 24, 30, 38 and 40 nm for loadings of 6.8%, 12.3%, 19.7% and 23.5 %, respectively. It has been reported that some facets of the semiconductors are more reactive in photoreduction or photooxidation compared to other facets,[50,51] although reports on reductive or oxidative facets of the same semiconductor crystal are inconsistent in literature. For example, Hotsenpiller et al. reported that photoreduction rate of Ag^+ is lower on the (001) and (110) facets compared to that on other facets of the rutile TiO_2 crystal,[52] while Farneth et al. concluded that Ag^+ ions are mostly photoreduced on the (110) face of rutile TiO_2.[53] Nevertheless, most of the reports on $BiVO_4$ crystal state that (010) is the most active facet for reduction[38,45,54] which is consistent with our observation. Our results show that when the concentration of silver in the precursor solution was increased, most of the (010) surface is cover by silver nanoparticles while the coverage on other facets is much less.

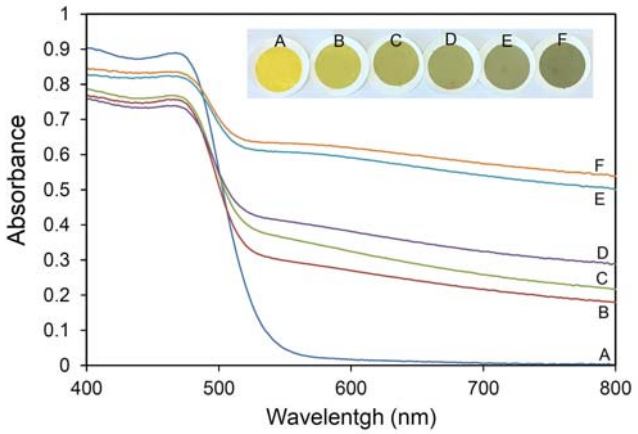

Figure 4. UV-Vis DRS of A) $BiVO_4$, B) Ag/$BiVO_4$-1.3%, C) Ag/$BiVO_4$-6.9%, D) Ag/$BiVO_4$-12.3%, E) Ag/$BiVO_4$-19.7%, and F) Ag/$BiVO_4$-23.5%. Inset: photo images of the corresponding samples showing the color change of $BiVO_4$ after deposition of silver.

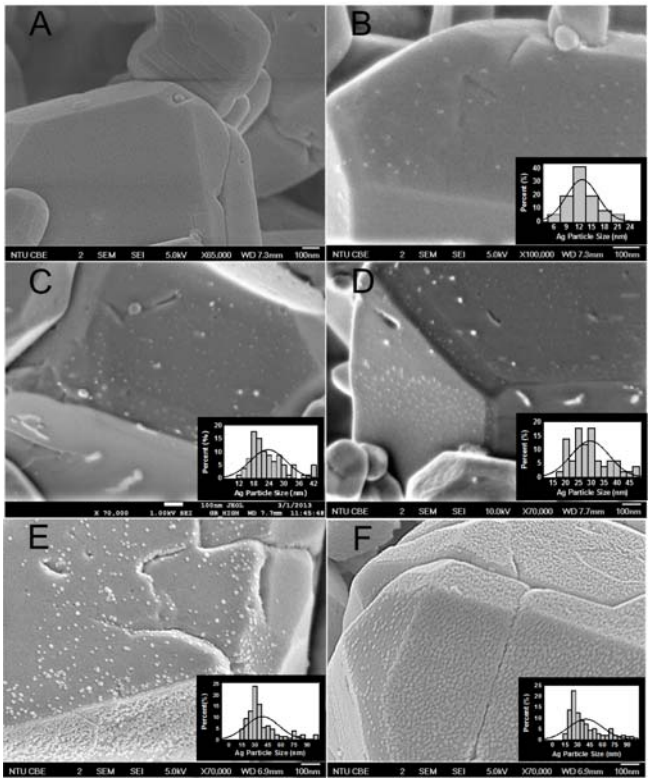

Figure 5. FESEM images of $BiVO_4$ with different percentage of silver after photodeposition. A) $BiVO_4$, B) Ag/$BiVO_4$-1.3%, C) Ag/$BiVO_4$-6.9%, D) Ag/$BiVO_4$-12.3%, E) Ag/$BiVO_4$-19.7%, and F) Ag/$BiVO_4$-23.5%. Inset: the size distribution of silver nanoparticles based on the measurement of 50 silver nanoparticles.

To further investigate chemical state of silver on the catalyst, sample Ag/$BiVO_4$-19.7% was analyzed by XPS and the results are

presented in Figure 6. Figure 6A shows the survey scan of both $BiVO_4$ and Ag/$BiVO_4$. The presence of Bi, V and O in both samples and Ag in Ag/$BiVO_4$ can be observed as expected. Figure 6B shows the high resolution spectrum of Bi 4f. Two peaks were detected with binding energies of 159.3 and 164.6 eV, corresponding to Bi $4f_{7/2}$ and Bi $4f_{5/2}$, respectively, of Bi^{3+} in $BiVO_4$. In Figure 6C, the peaks at 517.0 and 525.0 eV are attributed to V $2p_{3/2}$ and V $2p_{1/2}$ of V^{5+} in the sane oxide. The peak at 530.0 eV is assigned to O 1s. Figure 6D shows the spectrum of Ag 3d with the two peaks observed at 368.3 and 374.3 eV. They can be assigned to Ag $3d_{5/2}$ and Ag $3d_{3/2}$ of Ag^0, indicating that silver ions are readily reduced to metallic silver on $BiVO_4$ by photoreduction.[55]

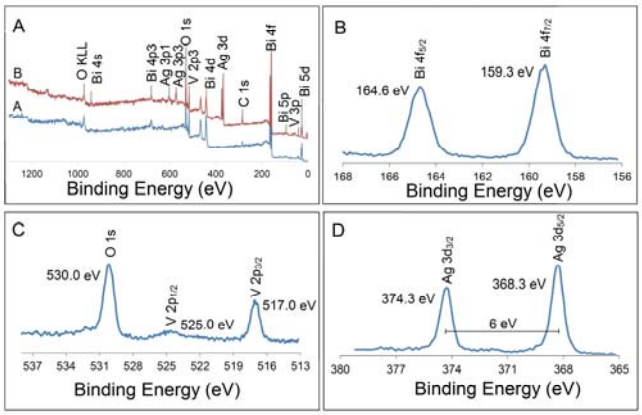

Figure 6. A) XPS survey scan of (A) $BiVO_4$ and (B) Ag/$BiVO_4$-19.7% and high resolution spectra of B) Bi 4f, C) V 2p and O 1s, and D) Ag 3d.

Disinfection performance of the photocatalysts

The photocatalytic disinfection activity of $BiVO_4$ and Ag/$BiVO_4$ was evaluated by inactivation of *E. coli* in aqueous buffer solution under visible light ($\lambda > 420$ nm). Control experiments showed that in the absence of the photocatalyst, *E. coli* cannot be inactivated both under visible light and in the dark. Figure 7A shows disinfection activity of $BiVO_4$ and Ag/$BiVO_4$ for *E. coli* under visible light. It can be seen that $BiVO_4$ alone has a low activity. After 6 h irradiation, the concentration of *E. coli* was only reduced to 4.5×10^5 CFU/mL. Low activity of $BiVO_4$ has been reported repeatedly in degradation of organic pollutants due to a fast recombination of photogenerated electron and hole pairs.[56-58] After deposition of silver nanoparticles on the surface of $BiVO_4$, significant increase in the activity can be observed. Control studies were also carried out under the same condition but in the dark. As shown in Figure 7B, in the absence of light, there were no significant changes in the concentration of bacterial cells, indicating that the inactivation of *E. coli* is mainly contributed by the photocatalytic process rather than the toxicity of silver nanoparticles. Figure 7A shows by increasing the percentage of silver, the photoactivity of the composite notably improves until the silver percentage reaches 19.7%. With this sample, it can be seen that all bacterial cells were killed within 3 h irradiation. Further increasing the silver content does not lead to much enhancement in the activity. Based on these results, Ag/$BiVO_4$ with 19.7 wt% of silver was chosen for the rest of the tests.

The stability of the photocatalyst was evaluated by using the same batch of photocatalyst sample in three consecutive runs of the disinfection tests. Figure 8 shows the disinfection activity of the photocatalyst in stability test. It can be seen that there is no significant difference in disinfection activity over the three runs. At the end of 3 h for all three runs, the bacterial cells were totally inactivated. ICP results showed no detectable changes in silver content of the photocatalyst after the three runs. Table 1 shows that the concentration of silver ions in the disinfection medium at the end of each run is in the range of 60-110 ppb (μg/L). Based on these data, the percentage of silver ions leached to the solution only accounts for 0.06% of silver in Ag/$BiVO_4$-19.7%. The low concentration of silver ions in the medium further supports that the disinfection activity is mainly due to the photocatalytic process since at such low concentrations of silver ions total disinfection takes as long as 24 h.[59,60]

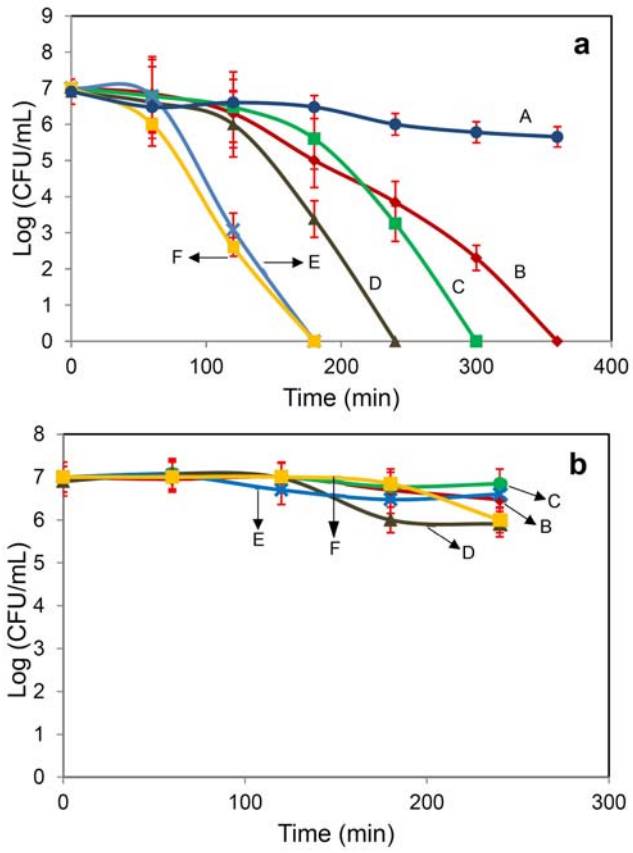

Figure 7. *E. coli* inactivation by A) $BiVO_4$, B) Ag/$BiVO_4$-1.3%, C) Ag/$BiVO_4$-6.9%, D) Ag/$BiVO_4$-12.3%, E) Ag/$BiVO_4$-19.7%, and F) Ag/$BiVO_4$-23.5%; (a) Under visible light ($\lambda > 420$ nm), (b) in the dark.

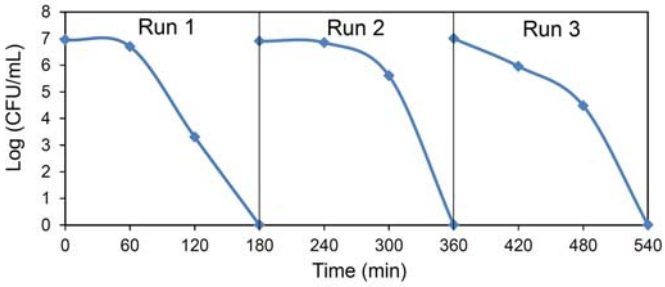

Figure 8. Stability of disinfection activity of Ag/$BiVO_4$-19.7% in three consecutive runs.

Table 1. The concentration of Ag^+ ions in the disinfection medium at the end each run during recycle study.

	[Ag^+] (ppb)
1st Run (5 h)	60
2nd Run (10 h)	110
3rd Run (15 h)	60

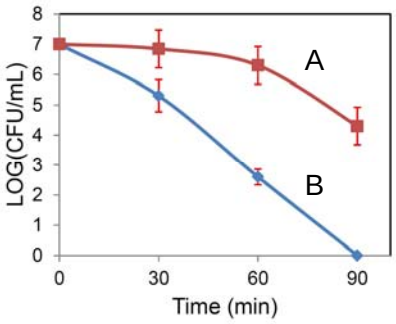

Figure 9. A) Control test without photocatalyst under sunlight, and B) antibacterial activity of $Ag/BiVO_4$ under sunlight.

The antibacterial test was also carried out outdoor under the afternoon Sun in Singapore. The photoactivity of $Ag/BiVO_4$ under the natural sunlight on *E. coli* is shown in Figure 9. It was observed that total disinfection occurred within 90 min. The rate of disinfection is almost doubled under natural sunlight compared to that under visible light ($\lambda > 420$ nm), which could be attributed to the UV content of the sunlight. As shown in Figure 9A, the natural sunlight alone has some disinfection effect on the bacterial cells.[61]

To reveal the disinfection mechanism, the concentrations of free radicals were measured. Figure 10A shows the fluorescent intensity of hTPA and Figure 10B shows the corresponding relative concentration of hydroxyl radical produced in the photocatalytic reaction. It can be observed that compared to $BiVO_4$ (curve A), samples deposited with silver nanoparticles all produce higher concentrations of hydroxyl radical. $Ag/BiVO_4$ with 19.7% of silver (Sample E) gives the highest concentration of hydroxyl radical. Figure 10C shows UV-Vis spectra of NBT after 30 min of irradiation and Figure 10D shows the corresponding relative concentration of the superoxide anion in the medium. It can be seen that the concentration of superoxide anion increases by increasing the percentage of silver on the surface of the catalyst, and reaches the maximum around 19.7% of silver loading. Such results are consistent with our photocatalytic antimicrobial activity data shown in Figure 7a. Based on these results, the mechanism of disinfection using silver nanoparticles deposited $BiVO_4$ is schematically shown in Figure 11. The main mechanism of action of the photocatalyst is the production of ROS.[13] Photocatalytic process has been widely reported effective in degrading organic and inorganic matters.[62-64] Hence, it is not surprising that photocatalytic process can damage cells which are made up of water and organic matters.[14] After the generation of photo-induced e^-/h^+ pairs, the holes can oxidize water and/or hydroxyl ions to generate the hydroxyl radical (•OH). The hydroxyl radical is a strong and nonselective oxidant that can degrade many types of biomolecules, including carbohydrates, nucleic acids, lipids, proteins, DNA and amino acids.[13] The electrons can react with the dissolved molecular oxygen through a reductive process to produce superoxide anion ($O_2•^-$) which is highly reactive and toxic to cell.[13] In this work, the deposition of silver nanoparticles on the surface of $BiVO_4$ is believed to greatly facilitate the e^-/h^+ separation based on the concentrations of free radicals detected and consistently the much enhanced photocatalytic antimicrobial activity.

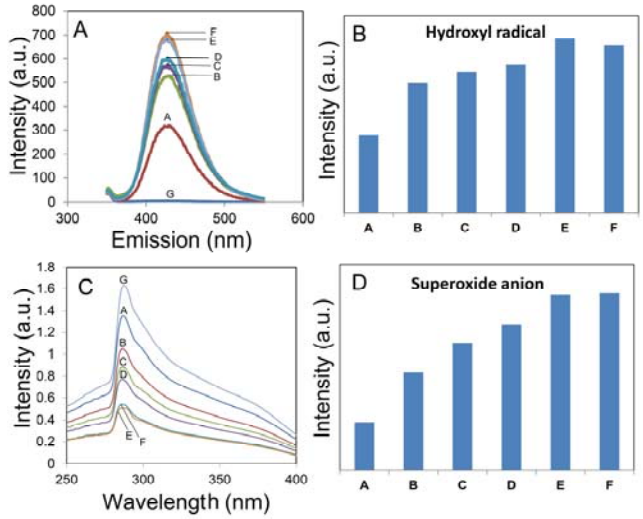

Figure 10. Detection of ROS after 30 min of irradiation in the presence of photocatalysts and probe molecules. A) fluorescence intensity of hTPA, B) relative concentration of hydroxyl radical produced, C) UV-Vis spectra of solutions with NBT, and D) relative concentration of superoxide anion produced. Curve G is from a control test without the catalyst; and the sample labels (A-F) for $Ag/BiVO_4$ follow the same order as those in Figure 3.

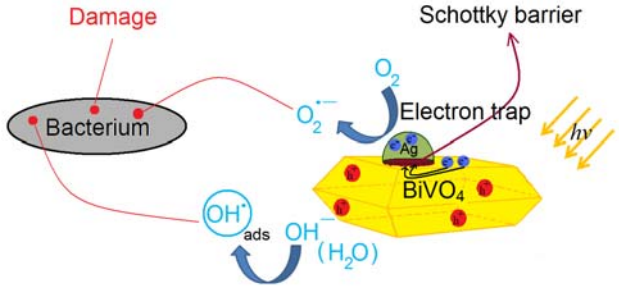

Figure 11. Schematic illustration of the disinfection mechanism based on $Ag/BiVO_4$.

It is well known that metal particles form an electron sink on the surface of semiconductor[65] which prevents the recombination of e^-/h^+ pair. When metal and semiconductor are brought into contact, Schottky barrier may form which is illustrated in Figure 12. In the case of n-type semiconductor, Schottky barrier height is the difference between interfacial conduction band (valance band in the case of p-type semiconductor) edge and Fermi level.[65] Schottky barrier height is equal to energy barrier that electron needs to pass to migrate from metal to semiconductor at their interface. Since metal has higher work function than semiconductor at metal/semiconductor interface, electrons will

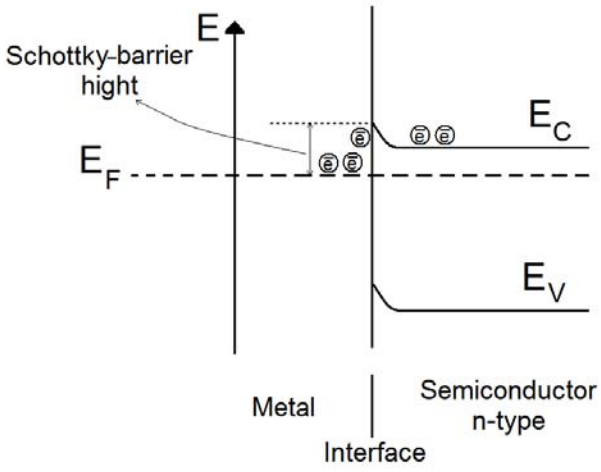

Figure 12. Schematic illustration of Schottky barrier (E_V and E_C are valance and conduction band potential, respectively, and E_F is pinned Fermi level).

naturally migrate from semiconductor to metal toward reaching the equilibrium chemical potential.[66] This phenomenon results in accumulation of excessive negative charges on the metal and excessive positive charges on the semiconductor at the interface. The excess positive charges force the electrons on the metal to migrate away from the barrier region. Schottky barrier formed at the interface of metal/semiconductor can lead to an efficient separation of e^-/h^+ pairs in photocatalytic process. It is expected that silver nanoparticles on $BiVO_4$ form a Schottky barrier at the interface, which enhances the photoactivity of the semiconductor significantly.[67] In general, increasing the loading of silver nanoparticles leads to more efficient separation of e^-/h^+ pairs. Nevertheless, in this study, it is found that when the loading of silver exceeds the optimum value of 19.7%, the activity is not further enhanced. This could be due to that under such a condition, light absorption and charge generation become the limiting step. This is further verified by the fact that the concentrations of hydroxyl radical and superoxide anion are not increased upon increasing the loading of silver beyond 19.7% (Figure 10). In addition, extra silver nanoparticles may become charge recombination centres.

Although there are many debates over the exact mechanism of degradation of bacteria exposed to the oxidative stresses caused by photocatalytic reaction, studies have shown that destruction of cell membrane is the main step in inactivation.[14] Figure 13A-C shows the images of damaged *E. coli* cells after photocatalytic disinfection together with the cell from the control experiment (Figure 13D). In contrast to the intact cells obtained from the control experiment, the damaged cells exhibit significant alteration of cell shape including rupture and collapse of the membrane which are the evidences of cell membrane dependent disinfection mechanism.

In view of the use of silver as one of the expensive metals in our system, a simple cost analysis is provided. Assume 1.3 wt% of silver is being considered as the lowest acceptable percentage of silver on the photocatalyst to have a satisfactory photoactivity. It

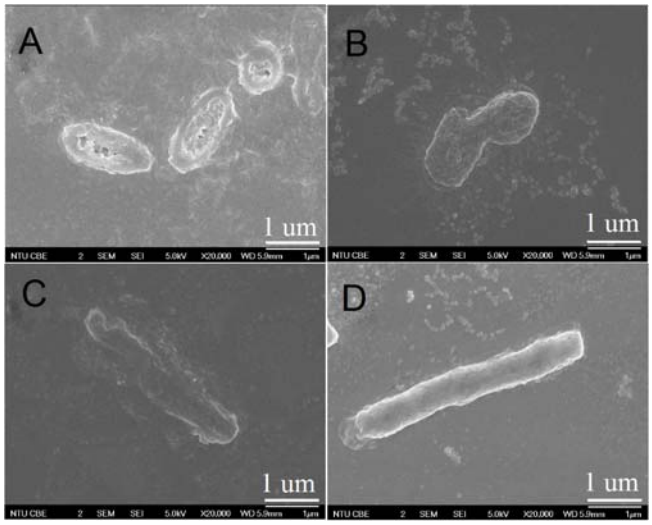

Figure 13. A, B and C) damaged cells due to photocatalytic disinfection after 3 h with 2 mg/mL of Ag/BiVO4-19.7% under visible light ($\lambda > 420$ nm), and D) Control cell, under the same condition but without photocatalyst and light.

takes 100 mg of $Ag/BiVO_4$ (19.7 wt% Ag) around 23000 h to reach this threshold based on our current experimental data. During this period, approximately 255 litres of water can be disinfected per 100 mg of $Ag/BiVO_4$. Based on the ICP result, the yield of silver deposition for production of $Ag/BiVO_4$-19.7% is 39%. Hence, the overall silver consumption is approximately 0.2 mg of silver per litre of water. Assuming a consumption of 4 L drinking water per day per person, the yearly silver consumption per person for drinking water production purpose is 292 mg. The price of silver is around US$0.8/g. Thus the silver cost incurred for the production of safe drinking water per person in each year is about US$0.24. The threshold limit of silver in drinking water is around 100 ppb specified by Environmental Protection Agency, USA. The detected concentration of silver ions in our reaction mixture is at the same magnitude. Nevertheless, silver ions need to be removed from water as much as possible in the long run. In our previous report, an effective adsorbent material based on carbon spheres synthesized from low-cost precursors has been developed which can adsorb silver ions in a stream with a low concentration efficiently.[68] By coupling this adsorption process with the photocatalytic disinfection process, silver concentration in the final product can be reduced even further.

Conclusions

In this study, silver nanoparticles were deposited on the micron-size $BiVO_4$ particles through a photocatalytic reduction process. UV-Vis analysis revealed a red shift on absorption edge upon deposition of silver on the semiconductor which increases by increasing the amount of silver. Photocatalytic activities of $Ag/BiVO_4$ have been evaluated by inactivation of *E. coli* in aqueous solution under visible light. It was found that photodeposition of silver on the $BiVO_4$ particles remarkably enhances the disinfection activity for *E. coli* compared to bare $BiVO_4$. The enhancement is attributed to the effect of silver

nanoparticles which promote the charge separation by trapping photo-generated electrons, leading to efficient production of reactive oxygen species. The fabricated Ag/$BiVO_4$ is shown to be a promising alternative for production of pathogen-free drinking water in areas with abundant sunlight.

Acknowledgements

This work is supported by Nanyang Technological University and Nanyang Environmental and Water Research Institute (NEWRI).

References

1. A. R. Morua, K. E. Halvorsen and A. S. Mayer, *Risk Analysis*, 2011, **31**, 866-878.
2. T. A. McDonald and H. Komulainen, *J. Environ. Sci. Health - Part C: Environ. Carcinog. Ecotoxicol. Rev.*, 2005, **23**, 163-214.
3. D. D. Ratnayaka, M. J. Brandt and K. M. Johnson, *Twort's Water Supply*, Butterworth-Heinemann, 2009.
4. J. Mansouri, S. Harrisson and V. Chen, *J. Mater. Chem.*, 2010, **20**, 4567-4586.
5. L. Villén, F. Manjón, D. García-Fresnadillo and G. Orellana, *Appl. Catal. B: Environ.*, 2006, **69**, 1-9.
6. T. Matsunaga, R. Tomoda, T. Nakajima and H. Wake, *FEMS Microbiol. Lett.*, 1985, **29**, 211-214.
7. C. McCullagh, J. M. C. Robertson, D. W. Bahnemann and P. K. J. Robertson, *Res. Chem. Intermediat.*, 2007, **33**, 359-375.
8. D. Y. Goswami, *Adv. Sol. Energy*, 1995, **10**.
9. S. Malato, J. Blanco, A. Vidal, D. Alarcón, M. I. Maldonado, J. Cáceres and W. Gernjak, *Sol. Energy*, 2003, **75**, 329-336.
10. S. Malato, J. Blanco, A. Vidal and C. Richter, *Appl. Catal. B: Environ.*, 2002, **37**, 1-15.
11. P. Fernández, J. Blanco, C. Sichel and S. Malato, *Catal. Today*, 2005, **101**, 345-352.
12. X. Chen and S. S. Mao, *Chem. rev.*, 2007, **107**, 2891-2959.
13. Y. Li, W. Zhang, J. Niu and Y. Chen, *ACS Nano*, 2012, **6**, 5164-5173.
14. O. K. Dalrymple, E. Stefanakos, M. A. Trotz and D. Y. Goswami, *Appl. Catal. B: Environ.*, 2010, **98**, 27-38.
15. E. J. Corey, M. M. Mehrotra and A. U. Khan, *Biochem. Bioph. Res. Co.*, 1987, **145**, 842-846.
16. H. Xu, H. Li, C. Wu, J. Chu, Y. Yan, H. Shu and Z. Gu, *J. Hazard. Mater.*, 2008, **153**, 877-884.
17. M. Zhang, C. Shao, X. Li, P. Zhang, Y. Sun, C. Su, X. Zhang, J. Ren and Y. Liu, *Nanoscale*, 2012, **4**, 7501-7508.
18. W. Wang, Y. Yu, T. An, G. Li, H. Y. Yip, J. C. Yu and P. K. Wong, *Environ. Sci. Technol.*, 2012, **46**, 4599-4606.
19. T. J. Haimei Fan, Lingling Wang, Dejun Wang, and P. W. Haiyan Li, dongqing he, Tengfeng Xie, *J. Phys. Chem.*, 2011.
20. Z. Zhou, M. Long, W. Cai and J. Cai, *J. Mol. Catal. A: Chem.*, 2012, **353–354**, 22-28.
21. J. Ren, W. Wang, S. Sun, L. Zhang and J. Chang, *Appl. Catal. B: Environ*, 2009, **92**, 50-55.
22. S.-W. Cao, Z. Yin, J. Barber, F. Y. C. Boey, S. C. J. Loo and C. Xue, *ACS Appl. Mater. Interfaces*, 2012, **4**, 418-423.
23. L. Zhu, C. He, Y. Huang, Z. Chen, D. Xia, M. Su, Y. Xiong, S. Li and D. Shu, *Sep. Purif. Technol.*, 2012, **91**, 59-66.
24. V. Brezová, A. Blažková, Ľ. Karpinský, J. Grošková, B. Havlínová, V. Jorík and M. Čeppan, *J. Photoch.Photobio. A*, 1997, **109**, 177-183.
25. A. Zhang and J. Zhang, *Appl. Surf. Sci.*, 2010, **256**, 3224-3227.
26. M. Pratap Reddy, A. Venugopal and M. Subrahmanyam, *Water Res.*, 2007, **41**, 379-386.
27. R. Georgekutty, M. K. Seery and S. C. Pillai, *J. Phys. Chem. C*, 2008, **112**, 13563-13570.
28. P. Wang, B. Huang, X. Qin, X. Zhang, Y. Dai, J. Wei and M.-H. Whangbo, *Angew. Chem. Int. Ed.*, 2008, **47**, 7931-7933.
29. S. Kohtani, J. Hiro, N. Yamamoto, A. Kudo, K. Tokumura and R. Nakagaki, *Catal. Commun*, 2005, **6**, 185-189.
30. K. J. A. Davies, *IUBMB Life*, 2000, **50**, 279-289.
31. M. Fedorova, N. Kuleva and R. Hoffmann, *J. Proteome Res.*, 2010, **9**, 2516-2526.
32. R. E. Pacifici and K. J. A. Davies, *Gerontology*, 1991, **37**, 166-180.
33. D. Ke, T. Peng, L. Ma, P. Cai and P. Jiang, *Appl. Catal. A: Gen.*, 2008, **350**, 111-117.
34. S. E. Page, W. A. Arnold and K. McNeill, *J. Environ. Monitor.*, 2010, **12**, 1658-1665.
35. L. Ye, J. Liu, Z. Jiang, T. Peng and L. Zan, *Appl. Catal. B: Environ.*, 2013, **142–143**, 1-7.
36. X. Xu, X. Duan, Z. Yi, Z. Zhou, X. Fan and Y. Wang, *Catal. Commun.*, 2010, **12**, 169-172.
37. D. Wang, H. Jiang, X. Zong, Q. Xu, Y. Ma, G. Li and C. Li, *Chem. Eur. J.*, 2011, **17**, 1275-1282.
38. S. Obregón, A. Caballero and G. Colón, *Appl. Catal. B: Environ.*, 2012, **117–118**, 59-66.
39. U. M. García Pérez, S. Sepúlveda-Guzmán, A. Martínez-de la Cruz and U. Ortiz Méndez, *J. Mol. Catal. A: Chem.*, 2011, **335**, 169-175.
40. M. Li, L. Zhao and L. Guo, *Int. J. Hydrogen Energ.*, 2010, **35**, 7127-7133.
41. D. Wang, R. Li, J. Zhu, J. Shi, J. Han, X. Zong and C. Li, *J. Phys. Chem. C*, 2012, **116**, 5082-5089.
42. C. Li, P. Zhang, R. Lv, J. Lu, T. Wang, S. Wang, H. Wang and J. Gong, *Small*, 2013, DOI: 10.1002/smll.201301276.
43. S. Sun, W. Wang, L. Zhou and H. Xu, *Ind. Eng. Chem. Res.*, 2009, **48**, 1735-1739.
44. H. Fan, D. Wang, L. Wang, H. Li, P. Wang, T. Jiang and T. Xie, *Appl. Surf. Sci.*, 2011, **257**, 7758-7762.
45. J. Yang , D. Wang , X. Zhou and C. Li, *Chem. Eur. J.*, 2013, **19**, 1320-1326.
46. C. Suwanchawalit, S. Wongnawa, P. Sriprang and P. Meanha, *Ceram. Int.*, 2012, **38**, 5201-5207.
47. L. Sun, J. Li, C. Wang, S. Li, Y. Lai, H. Chen and C. Lin, *J. Hazard. Mater.*, 2009, **171**, 1045-1050.
48. H. A. Atwater and A. Polman, *Nat. Mater.*, 2010, **9**, 205-213.
49. S. K. Cushing, J. Li, F. Meng, T. R. Senty, S. Suri, M. Zhi, M. Li, A. D. Bristow and N. Wu, *J. Am. Chem. Soc.*, 2012, **134**, 15033-15041.
50. J. Pan, G. Liu, G. Q. Lu and H.-M. Cheng, *Angew. Chem. Int. Ed.*, 2011, **50**, 2133-2137.
51. H. G. Yang, C. H. Sun, S. Z. Qiao, J. Zou, G. Liu, S. C. Smith, H. M. Cheng and G. Q. Lu, *Nature*, 2008, **453**, 638-641.
52. P. A. Morris Hotsenpiller, J. D. Bolt, W. E. Farneth, J. B. Lowekamp and G. S. Rohrer, *J. Phys. Chem. B*, 1998, **102**, 3216-3226.
53. W. E. Farneth, R. S. McLean, J. D. Bolt, E. Dokou and M. A. Barteau, *Langmuir*, 1999, **15**, 8569-8573.
54. Rengui Li, Fuxiang Zhang, Donge Wang, Jingxiu Yang, Mingrun Li, Jian Zhu, Xin Zhou, H. Han and C. Li, *Nat. Commun.*, 2013.
55. John F. Moulder, William F. Stickle, Peter E. Sobol and Kenneth D. Bomben, *Handbook of X-ray Photoelectron Spectroscopy (Edited by J. Chastain)*, Perkin-Elmer Corporation, 1992.
56. L. Xigiang, Z. Xiufang, D. Xiaoli, M. Chun, Z. Xinxin and M. Hongchao, in *1st International Conference on Energy and Environmental Protection (ICEEP 2012), 23-24 June 2012*, Trans Tech Publications Ltd., Switzerland, 2012, pp. 732-735.
57. K. Liu, Z. Chang, W. Li, P. Che and H. Zhou, *Sci. China Chem.*, 2012, **55**, 1770-1775.
58. Y.-H. Xu, C.-J. Liu, M.-J. Chen and Y.-Q. Liu, *Int. J. Nanoparticles*, 2011, **4**, 268-283.
59. M. A. Butkus, L. Edling and M. P. Labare, *J. Water Supply: Res. T.*, 2003, **52**, 407-416.
60. J. H. Cunningham, C. Cunningham, B. V. Aken and L.-S. Lin, *Water Sci. Technol.*, 2008, **58**, 937-944.
61. K. G. McGuigan, T. M. Joyce and R. M. Conroy, *J. Med. Microbiol.*, 1999, **48**, 785-787.
62. M. N. Chong, B. Jin, C. W. K. Chow and C. Saint, *Water Res.*, 2010, **44**, 2997-3027.
63. M. R. Hoffmann, S. T. Martin, W. Choi and D. W. Bahnemann, *Chem. Rev.*, 1995, **95**, 69-96.
64. D. S. Bhatkhande, V. G. Pangarkar and A. A. C. M. Beenackers, *J. Chem. Technol. Biotechnol.*, 2002, **77**, 102-116.
65. R. T. Tung, *Mater. Sci. Eng. R Rep.*, 2001, **35**, 1-138.
66. Z. Shan, J. Wu, F. Xu, F.-Q. Huang and H. Ding, *J. Phys. Chem. C*, 2008, **112**, 15423-15428.
67. X. Zhang, Y. Zhang, X. Quan and S. Chen, *J. Hazard. Mater.*, 2009, **167**, 911-914.
68. X. Song, P. Gunawan, R. Jiang, S. S. J. Leong, K. Wang and R. Xu, *J. Hazard. Mater.*, 2011, **194**, 162-168.